SCIENTIFIC REP⚙RTS

OPEN

Low-Frequency Raman Spectroscopy of Few-Layer 2H-SnS₂

Tharith Sriv[1,2], Kangwon Kim[1] & Hyeonsik Cheong [ID][1]

We investigated interlayer phonon modes of mechanically exfoliated few-layer 2H-SnS₂ samples by using room temperature low-frequency micro-Raman spectroscopy. Raman measurements were performed using laser wavelengths of 441.6, 514.4, 532 and 632.8 nm with power below 100 μW and inside a vacuum chamber to avoid photo-oxidation. The intralayer E_g and A_{1g} modes are observed at ~206 cm^{-1} and 314 cm^{-1}, respectively, but the E_g mode is much weaker for all excitation energies. The A_{1g} mode exhibits strong resonant enhancement for the 532 nm (2.33 eV) laser. In the low-frequency region, interlayer vibrational modes of shear and breathing modes are observed. These modes show characteristic dependence on the number of layers. The strengths of the interlayer interactions are estimated by fitting the interlayer mode frequencies using the linear chain model and are found to be 1.64×10^{19} N·m^{-3} and 5.03×10^{19} N·m^{-3} for the shear and breathing modes, respectively.

Interest in two-dimensional (2D) materials such as hexagonal boron nitride (hBN), black phosphorus (BP) and transition-metal dichalcogenides (TMDs) since the discovery[1] of graphene in 2004 has significantly increased due to their unique structures and properties. Most TMD materials such as MoS(e)₂ and WS(e)₂ are indirect band gap semiconductors with band gap energies in the visible range but become direct in the monolayer limit[2–6]. Recently, tin disulfide (SnS₂) has attracted much interest because it is recognized as earth-abundant, relatively cheap and low-toxic material. Additionally, it has been shown to have high on/off current ratios for field effect transistors[7,8], fast photodetection[9] suitable for flexible photodetectors from UV to IR[10], interesting gas sensing property[11], and high optical absorption and photovoltaic activities[12].

SnS₂ is among the most important sulfide compounds of tin[13,14] and has more than 70 polytypes[13–15] differing from one another by stacking sequences of the individual sandwiched layers. The most common one is 2H-SnS₂ whose basic layer consists of a sheet of close-packed tin atoms sandwiched between two sheets of sulfur atoms[16–32]. It should be noted that in the literature, SnS₂ with a structure identical to that of 1T-MoS₂ as shown in Fig. 1(a) is called 2H-SnS₂[17–32], which should not be confused with the structure of 2H-MoS₂. In 2H-SnS₂, a metal atom is octahedrally coordinated by sulfur atoms, whereas the metal atom in 2H-MoS₂ possesses trigonal prismatic coordination[16]. Monolayers of 2H-SnS₂ are stacked exactly on top of one another to form 2H-polytype of bulk SnS₂. Between the neighboring layers of 2H-SnS₂, there exists weak van-der-Waals interaction[33] offering easy mechanical cleavage along the c-axis down to monolayer. Bulk 2H-SnS₂ belongs to the symmetry group of $D_{3d}^3 (P\bar{3}m1)$ and has a trigonal structure with the lattice constants of $a = 3.6486$ Å and $c = 5.8992$ Å[17]. Unlike most TMDs, 2H-SnS₂ is projected to remain an indirect band gap semiconductor for all thicknesses, with the band gap ranging between 2.18 eV (bulk) and 2.41 eV (monolayer). Although chemical vapor deposition[34] and molecular beam epitaxy[35] growths have been tried, large-area growth of few-layer SnS₂ has not been realized yet. At the moment, mechanical exfoliation from bulk crystals yields the highest quality few-layer samples.

Raman spectroscopy is one of the most widely used characterization tools for 2D layered materials to determine the number of layers as well as polytypes or strain effects. More importantly, one can use low-frequency Raman spectroscopy to study the interlayer interactions of few-layer materials by measuring the in-plane (shear) and out-of-plane (breathing) modes in the low-frequency region (<50 cm^{-1}). In the literature, the measured data of the shear and breathing modes are used to estimate the interlayer spring constants of the studied materials such as MoS₂ and WSe₂[36], MoSe₂[37], MoTe₂[38], WS₂[39], ReS(e)₂[40], Bi₂Te₃ and Bi₂Se₃[41], black phosphorus[42], and graphite[43,44] by fitting the experimental data to the linear chain model (LCM). Additionally, Luo et al. reported that the

¹Department of Physics, Sogang University, Seoul, 04107, Korea. ²Department of Physics, Royal University of Phnom Penh, Phnom Penh, Cambodia. Correspondence and requests for materials should be addressed to H.C. (email: hcheong@sogang.ac.kr)
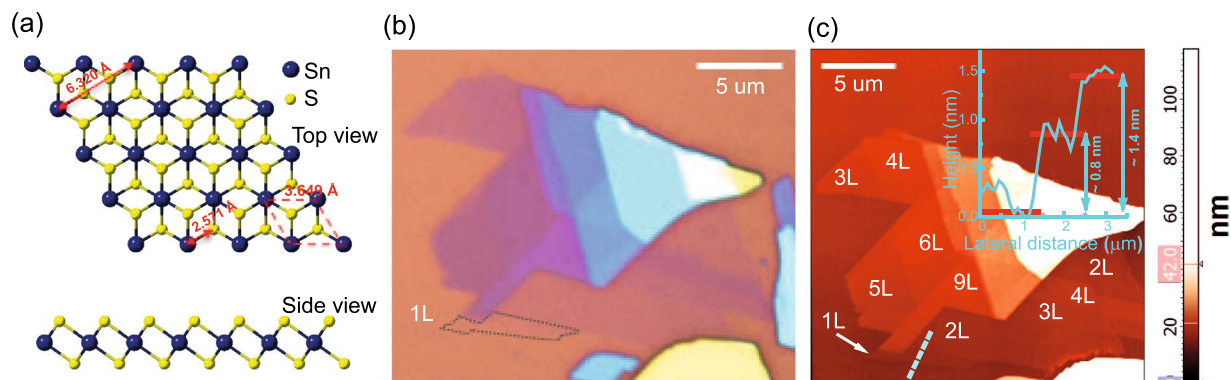
Figure 1. (**a**) Crystal structure of monolayer 2H-SnS$_2$. (**b**) Optical and (**c**) atomic force microscope (AFM) images of a mechanically exfoliated few-layer 2H-SnS$_2$ sample on a SiO$_2$/Si substrate.

stacking sequence determines Raman intensities of observed interlayer shear modes[45]. However, experimental work on Raman properties of few-layer 2H-SnS$_2$ remains lacking although results for less-common 4H-SnS$_2$ have been reported[19]. The Raman spectrum of bulk 2H-SnS$_2$ shows two phonon modes at 315 cm^{-1} (A_{1g}) and 205.5 cm^{-1} (E_g), while that of 4H-SnS$_2$ shows several more modes[26]. This offers a clear distinction between 2H- and 4H-SnS$_2$. For few-layer SnS$_2$, Yuan et al.[19] recently reported a Raman study on mechanically-exfoliated monolayer and few-layer as well as bulk 4H-SnS$_2$. Nevertheless, low-frequency shear and breathing modes are not considered, i.e., interlayer interactions of the material remains uncovered in the Raman studies of few-layer SnS$_2$. In this work, we investigate the Raman spectra of mechanically-exfoliated few-layer 2H-SnS$_2$ using four excitation energies. We also analyze the low-frequency Raman spectra to investigate the interlayer interaction in few-layer 2H-SnS$_2$.

Results and Discussion

Figure 1(b,c) show the optical and AFM images of a 2H-SnS$_2$ sample, respectively. The dotted outline in Fig. 1(b) indicates where monolayer (1L) is located. The AFM measurements of this sample indicate the presence of several thicknesses as indicated. The 1 L 2H-SnS$_2$ has a thickness of ~0.6 nm[19]. Our AFM results show a step size of ~0.8 nm for 1 L and ~1.4 nm for 2L, which is reasonable as there usually is a small extra thickness for the first layer in AFM measurements of 2D materials. This is either due to trapping of absorbed H$_2$O molecules between the 2H-SnS$_2$ and the SiO$_2$/Si substrate[19] or imperfect adhesion of the sample on the substrate. We measured multiple sets of samples with thicknesses ranging from 1L to 14L and bulk. It is worth mentioning that no sign of degradation was observed after our few-layer 2H-SnS$_2$ samples had been left in ambient condition for several weeks, but AFM measurements performed few hours after being exposed to the laser beam in the Raman measurements in ambient air showed degradation caused by photo-oxidation (see Supplementary Information). We therefore carried out all Raman measurements with the sample kept inside a vacuum chamber.

Figure 2(a) shows the low- and high-frequency Raman spectra of 5L 2H-SnS$_2$ measured with four excitation energies. Vertical dashed-lines are guides for the eye. It is seen that the Raman signals are strongest for the 2.33 eV (532 nm) excitation laser. The out-of-plane A_{1g} mode at ~314 cm^{-1} is most prominent. The E_g mode at ~206 cm^{-1} is extremely weak and is barely resolved only in the spectrum taken with the excitation energy of 2.81 eV (441.6 nm). In the low-frequency region, the interlayer vibrational modes of in-plane shear (S) and out-of-plane breathing (B) modes are identified. Figure 2(b) shows the excitation energy dependence of the A_{1g} mode for 1L to 14L 2H-SnS$_2$. The 532 nm (2.33 eV) excitation laser provides the strongest intensity of the A_{1g} mode, which implies that the band gap of few-layer 2H-SnS$_2$ may be smaller than the recent theoretical prediction of 2.41 eV for 1L[16]. Figure 2(c) shows the dependence of the Raman spectrum on the number of layers. In addition to the A_{1g} and E_g modes, two other weak signals from A_{1u} and A_{1g}-LA (M) modes are observed for bulk or thick samples at ~353 cm^{-1} and ~140 cm^{-1}, respectively. The A_{1u} mode is an infrared mode but appear probably due to activation by lattice disorders, whereas the two-phonon scattering[46,47] signal of A_{1g}-LA (M) is weak due to the small scattering cross section. Figure 2(d) shows the E_g mode measured with the 441.6 nm excitation laser in cross polarization configuration since this excitation laser provided relatively stronger signals for the E_g mode. No clear shift is observed as the thickness increases. Figure 2(e) indicates the evolution of the Raman intensity and the peak position of the A_{1g} mode as a function of the number of layers. The error bars indicate the spectral resolution of the setup. The intensity of the A_{1g} mode evolves monotonically with the number of layers up to ~11L. This mode also shows a slight blue-shift from 1L to 3L, which is in good agreement with recent theoretical results[16].

For 1L 2H-SnS$_2$, there exist nine vibrational modes at the center of the Brillouin zone at the Γ point: $\Gamma = A_{1g} + E_g + 2A_{2u} + 2E_u$[20,26]. Among six optical phonon modes, there are three Raman active modes (A_{1g} and E_g) and three infrared-active modes (A_{2u} and E_u). The three acoustic modes belong to A_{2u} and E_u. The Raman scattering intensity is proportional to $|e_i \cdot \widetilde{R} \cdot e_s|$, where e_i represents the polarization vector of the incident light, e_s that of the scattered light, and $\widetilde{R}$ the Raman tensor. The Raman tensors can be expressed as[48],
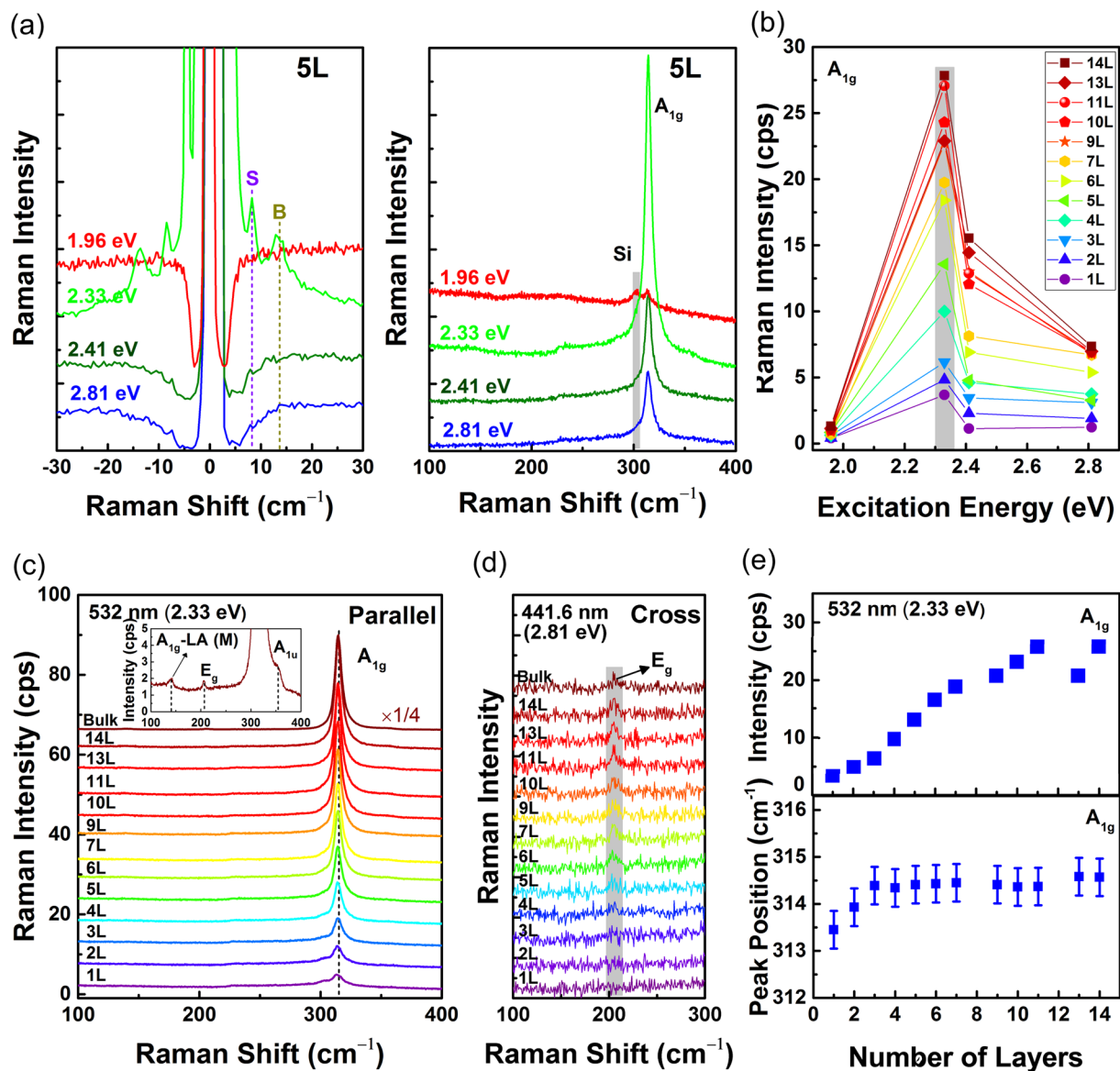
Figure 2. Raman spectra of few-layer 2H-SnS$_2$. (**a**) Low- and high-frequency modes of 5L 2H-SnS$_2$ measured with 441.6, 514.4, 532 and 632.8 nm lasers. (**b**) Excitation-energy dependence of the intensity of the A_{1g} mode for 1L to 14L. (**c**) High-frequency modes of few-layer 2H-SnS$_2$ measured by using the 532 nm laser in parallel polarization configuration. The Raman intensity of A_{1g} mode in bulk layer is multiplied by 1/4. Inset shows the A_{1g}-LA (M), E_g, and A_{1u} modes of bulk 2H-SnS$_2$. (**d**) The E_g mode measured by using the 441.6 nm laser in cross polarization configuration. (**e**) Evolution of the Raman intensity and peak positions of the A_{1g} mode as a function of number of layers. The error bars indicate the spectral resolution of the setup.

$$A_{1g} = \begin{pmatrix} a & 0 & 0 \\ 0 & a & 0 \\ 0 & 0 & b \end{pmatrix} \text{ and } E_g = \begin{pmatrix} c & 0 & 0 \\ 0 & -c & d \\ 0 & d & 0 \end{pmatrix}, \begin{pmatrix} 0 & -c & -d \\ -c & 0 & 0 \\ -d & 0 & 0 \end{pmatrix} \tag{1}$$

In the backscattering geometry with the laser propagating in the z direction, only the E_g mode is observable in cross polarization, whereas both the A_{1g} and E_g modes can be observed in parallel polarization configuration. For the low-frequency interlayer modes that exist in 2L or thicker 2H-SnS$_2$, the shear modes correspond to E_g and the breathing modes A_{1g}. By using polarized Raman measurements, one can thus distinguish shear and breathing modes unequivocally.

Figure 3(a) illustrates the polarization dependence of the Raman spectrum of 5L 2H-SnS$_2$. As a function of the relative scattering polarization angle with respect to the incident polarization direction, the intensities of the intralayer A_{1g} mode and the interlayer breathing modes are modulated, whereas the intralayer E_g mode and the interlayer shear modes are independent of the scattering polarization, which is consistent with the Raman
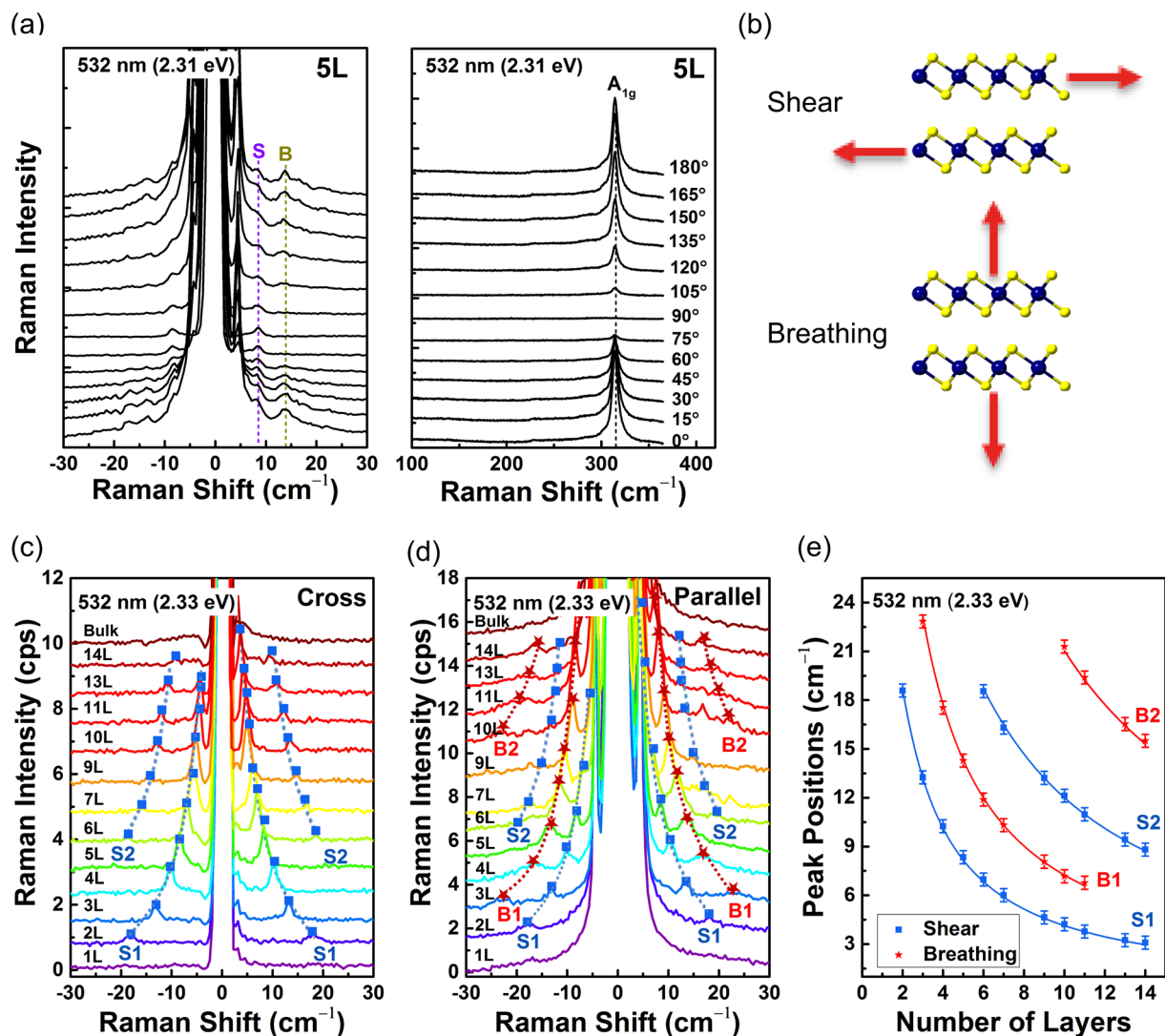
Figure 3. (**a**) Scattering angle dependence of the Raman spectra of 5L 2H-SnS2 measured by using 2.33 eV (532 nm) excitation laser. Labels S (shear) and B (breathing) indicate the positions of shear and breathing modes resolved in 5L 2H-SnS2, respectively. (**b**) Schematics of interlayer in-plane shear and out-of-plane breathing modes. (**c**) Shear modes measured in cross polarization. (**d**) Shear and breathing modes measured in parallel polarization. The dashed curves are guides for the eye. (**e**) Peak positions as a function of number of layers. Solid curves are fitting results using the linear chain model.

tensor analysis above. Figure 3(b) illustrates the vibrations of in-plane shear and out-of-plane breathing. The evolution of the low-frequency interlayer vibrational modes as a function of the number of layers is shown in Fig. 3(c–e). The shear and breathing modes can be distinguished by using polarized Raman measurements as explained before. Figure 3(c) shows the shear modes measured in cross polarization, in which the breathing modes are suppressed. Up to 2 shear modes (S1 and S2) are identified, and their positions depend sensitively on the number of layers. Figure 3(d) shows similar spectra measured in parallel polarization. Here, both the shear and breathing modes are observed. By comparing with Fig. 3(c), one can unambiguously identify the breathing modes (B1 and B2). Figure 2(e) summarizes the evolution of the interlayer vibrational modes as a function of the number of layers. Since the high-frequency intralayer modes show little dependence on the number of layers beyond 3L, low-frequency Raman analysis would be the most reliable method to determine the number of layers of few-layer 2H-SnS2.

As the low-frequency interlayer modes reflect the strength of the interlayer interaction, one can estimate the interlayer spring constants in the in-plane and out-of-plane directions by analyzing the frequencies of the shear and breathing modes, respectively. In the linear chain model[36,41,49], assuming that only interactions between nearest-neighbor layers are important and by neglecting the substrate and surface effects, the angular frequency of the α-th shear (breathing) mode in N-layer 2H-SnS2 is given by,

Material	K_S (10^{19} N·m^{-3})	K_B (10^{19} N·m^{-3})
SnS$_2$ (this work)	1.64	5.03
MoS$_2$[36]	2.72	8.62
MoSe$_2$[37]	2.92	8.73
MoTe$_2$[38]	3.44	7.83
WS$_2$[39]	2.99	9.10
WSe$_2$[36]	3.07	8.63
ReS$_2$[40]	1.71/1.89	6.90
ReSe$_2$[40]	1.78/1.94	6.90
Bi$_2$Te$_3$[41]	4.57	13.33
Bi$_2$Se$_3$[41]	2.27	5.26
Black phosphorus[42]	—	12.3
Graphite[43,44]	1.20	9.40

Table 1. Force constants per unit area of 2H-SnS$_2$ obtained by fitting experimental data to the linear chain model and comparison with those of other TMD materials.

$$\omega_\alpha = \frac{1}{\pi c} \sqrt{\frac{K}{2\mu}\left[1 - \cos\left(\frac{(\alpha - 1)\pi}{N}\right)\right]},$$

(2)

where $\alpha = 2, 3, \ldots, N$ ($\alpha = 1$ corresponds to the zero-frequency acoustic mode at Γ point in the Brillouin zone), c is the speed of light in vacuum, K is the in-plane (out-of-plane) force constant, and $\mu = 2.63352 \times 10^{-26}$ kg · Å^{-2} is the mass per unit area of monolayer of 2H-SnS$_2$. The in-plane ($K = K_S$) and out-of-plane ($K = K_B$) force constants per unit area can then be obtained by fitting the experimentally obtained peak frequencies of the shear and breathing modes, respectively, to equation (2). Table 1 compares the force constants per unit area of 2H-SnS$_2$ thus obtained with those of other layered materials found in the literature. The interlayer interaction in 2H-SnS$_2$ is significantly weaker than in most materials compared.

In summary, we investigated lattice dynamics of mechanically-exfoliated few-layer 2H-SnS$_2$ by room temperature low-frequency micro-Raman spectroscopy using four different excitation energies. In monolayer, the intralayer out-of-plane A_{1g} (~314 cm^{-1}) mode is most prominent, whereas in thick samples and bulk, the weak in-plane E_g (~206 cm^{-1}) mode as well as two additional modes such as $A_{1g} - LA(M)$ (~140 cm^{-1}) and A_{1u} (~353 cm^{-1}) are resolved. The 2.33 eV (532 nm) excitation laser provides the strongest Raman signals of intralayer A_{1g} mode and interlayer shear and breathing modes, whereas the E_g mode appears stronger for the 2.81 eV (441.6 nm) excitation. For the A_{1g} mode, the Raman shift is slightly sensitive to thickness for 1L-3L, but not for thicker material. The shear and breathing modes show strong dependence on the thickness, which provides a robust criterion for determination of the thickness using Raman spectroscopy. The interlayer interactions obtained by analyzing the interlayer vibrational modes are weaker than in most other layered materials. These results provide valuable information on materials parameters for device designs using few-layer 2H-SnS$_2$.

Methods

Few-layer 2H-SnS$_2$ samples were prepared from a SnS$_2$ single-crystal (HQ Graphene) onto SiO$_2$/Si substrates with 280 nm-thick oxide layer by mechanical exfoliation. The thickness of the samples was determined by atomic force microscope (AFM) and further confirmed by Raman measurements. The AFM measurements were performed by using a commercial AFM system (NT-MDT NTEGRA Spectra). Room temperature micro-Raman spectroscopy was conducted in backscattering geometry using four different excitation energies: the 441.6 nm (2.81 eV) line of a He-Cd laser, the 514.4 nm (2.41 eV) line of a diode-pumped laser (Cobolt), the 532 nm (2.33 eV) line of a diode-pumped solid-state (DPSS) laser, and the 632.8 nm (1.96 eV) line of a He-Ne laser. The input laser beam was focused onto the samples by a 40× microscope objective lens (0.6 NA), and the scattered light was collected and collimated by the same objective lens. The laser of power below 100 μW was used. All measurements were performed with the sample in a vacuum chamber to prevent photo-oxidation. AFM images [Supplementary Information Fig. S1] taken after Raman measurements confirmed that there were no apparent damages. Volume holographic filters (Ondax and OptiGrate) were used to access the low-frequency range below 50 cm^{-1}. The Raman scattering signals were dispersed by a Jobin-Yvon iHR550 spectrometer with a 2400 grooves/mm grating (400 nm blaze) and detected by a liquid-nitrogen-cooled back-illuminated charged-couple-device (CCD) detector. The spectral resolution was below 1 cm^{-1}.

References

1. Novoselov, K. S. et al. Electric field effect in atomically thin carbon films. Science **306**, 666–669 (2004).
2. Liu, H. et al. High-harmonic generation from an atomically thin semiconductor. Nat. Phys. **13**, 263–266 (2016).
3. Zhang, X. X. et al. Magnetic brightening and control of dark excitons in monolayer WSe$_2$. Nat. Nanotech. **12**, 883–889 (2017).
4. Yan, T., Ye, J., Qiao, X., Tan, P. & Zhang, X. Exciton valley dynamics in monolayer WSe$_2$ probed by the two-color ultrafast Kerr rotation. Phys. Chem. Chem. Phys. **19**, 3176–3181 (2017).
5. Cui et al. Low-temperature Ohmic contact to monolayer MoS$_2$ by van der Waals bonded Co-h-BN electrodes. Nano Lett. **17**, 4781–4786 (2017).
6. Chen, S. Y., Zheng, C., Fuhrer, M. S. & Yan, J. Helicity-resolved Raman scattering of MoS$_2$, MoSe$_2$, WS$_2$, and WSe$_2$ atomic layers. Nano Lett. **15**, 2526–2532 (2015).

7. Song, H. S. *et al*. High-performance top-gated monolayer SnS$_2$ field effect transistors and their integrated logic circuits. *Nanoscale* **5**, 9666–9670 (2013).

8. De, D. *et al*. High on/off ratio field effect transistors based on exfoliated crystalline SnS$_2$ nano-membranes. *Nanotechnology* **24**, 025202 (2013).

9. Su, G. *et al*. Chemical vapor deposition of thin crystals of layered semiconductor SnS$_2$ for fast photodetection application. *Nano Lett.* **15**, 506–513 (2014).

10. Tao, Y., Wu, X., Wang, W. & Wang, J. Flexible photodetector from ultraviolet to near infrared based on a SnS$_2$ nanosheet microsphere film. *J. Mater. Chem. C* **3**, 1347–1353 (2015).

11. Shi, W. *et al*. Hydrothermal growth and gas sensing property of flower-shaped SnS$_2$ nanostructures. *Nanotechnology* **17**, 2918–2924 (2006).

12. Cui, X., Xu, W., Xie, Z. & Wang, Y. High-performance dye-sensitized solar cells based on Ag-doped SnS$_2$ counter electrodes. *J. Mater. Chem. A* **4**, 1908–1914 (2016).

13. Gopalakrishman, P., Anbazhagan, G., Vijayarajasekaran, J. & Vijayakumar, K. Effect of substrate temperature on tin disulphide thin films. *Int. J. Thin. Fil. Sci. Tec.* **6**, 73–75 (2017).

14. Gou, X. L., Chen, J. & Shen, P. W. Synthesis characterization and application of SnS$_x$ (x = 1,2) nanoparticles. *Mater. Chem. and Phys.* **93**, 557–566 (2005).

15. Price, L. S. *et al*. Atmospheric pressure chemical vapor deposition of tin sulfides (SnS, Sn$_2$S$_3$, and SnS$_2$) on glass. *Chem. Mater.* **11**, 1792–1799 (1999).

16. Gonzalez, J. M. & Oleynik, I. I. Layer-dependent properties of SnS$_2$ and SnSe$_2$ novel two-dimensional materials. *Phys. Rev. B* **94**, 125443 (2016).

17. Mitchell, R. S., Fujiki, Y. & Ishizawa, Y. Structural polytypism of SnS$_2$. *Nature* **247**, 537–538 (1974).

18. Burton, L. A. *et al*. Electronic and optical properties of single crystal SnS$_2$: an earth-abundant disulfide photocatalyst. *J. Mater. Chem. A* **4**, 1312–1318 (2016).

19. Huang, Y. *et al*. Tin disulfide: An emerging layered metal dichalcogenide semiconductor- materials properties and device characteristics. *ACS Nano* **8**, 10743–10755 (2014).

20. Utyuzh, A. N., Timofeev, Y. A. & Stepanov, G. N. Effect of pressure on Raman spectra of SnS$_2$ single crystals. *Phys. of Solid State* **52**, 352–356 (2010).

21. Mitchell, R. S., Fujiki, Y. & Ishizawa, Y. Structural polytypism of tin disulfide: its relationship to environments of formation. *J. Crystal Growth* **57**, 273–279 (1982).

22. Mikkelsen, J. C. Polytype characterization of SnS$_2$ crystal grown from Sn-rich melts. *J. Crystal Growth* **49**, 253–260 (1980).

23. Palosz, B., Palosz, W. & Gierlotka, S. Polytypism of crystals of tin disulphide; Structures of 21 polytypes of SnS$_2$. *Acta Crystallogr. C* **41**, 807–811 (1985).

24. Whitehouse, C. R. & Balchin, A. A. Polytypism in tin disulphide. *J. Crystal Growth* **47**, 203–212 (1979).

25. Powell, M. J., Liang, W. Y. & Chadi, D. J. Pressure dependence of the band structure of 2H-SnS$_2$. *J. Phys. C: Solid State Phys.* **11**, 885–894 (1978).

26. Smith, A. J., Meek, P. E. & Liang, W. Y. Raman scattering studies of SnS$_2$ and SnSe$_2$. *J. Phys. C: Solid State Phys.* **10**, 1321–1333 (1977).

27. Katahama, H., Nakashima, S., Mitsuishi, A., Ishigame, M. & Arashi, H. Raman scattering study of interlayer bonding in CdI$_2$ and SnS$_2$ under hydrostatic pressure: analysis by use of van der Waals interaction. *J. Phys. Chem. Solids* **44**, 1081–1087 (1983).

28. Palosz, B., Steurer, W. & Schulz, H. Refinement of SnS$_2$ polytypes 2H, 4H and 18R. *Acta Crystallogr.* **B46**, 449–455 (1990).

29. Acharya, S. & Srivastava, O. N. Electronic behaviour of SnS$_2$ crystals. *Phys. Stat. Sol.* **65**, 717–723 (1981).

30. Palosz, B. & Salje, E. Lattice parameters and spontaneous strain in AX$_2$ polytypes: CdI$_2$, PbI$_2$, SnS$_2$ and SnSe$_2$. *J. Appl. Cryst.* **22**, 622–623 (1989).

31. Shibata, T., Muranushi, Y., Miura, T. & Kishi, T. Photoconductive properties of single crystal 2H-SnS$_2$. *J. Phys. Chem. Solids* **51**, 1297–1300 (1990).

32. Shibata, T., Kambe, N., Muranushi, Y., Miura, T. & Kishi, T. Optical characterisation of single crystal 2H-SnS$_2$ synthesised by the chemical vapour transport method at low temperatures. *J. Phys. D: Appl. Phys.* **23**, 719–723 (1990).

33. Ahn, J. H. *et al*. Deterministic two-dimensional polymorphism growth of hexagonal n-type SnS$_2$ and orthorhombic p-type SnS crystals. *Nano Lett.* **15**, 3703–3708 (2015).

34. Wang, Z. & Pang, F. In-plane growth of large ultra-thin SnS$_2$ nanosheets by tellurium-assisted chemical vapor deposition. *RSC Adv.* **7**, 29080–29087 (2017).

35. Schlaf, R. Molecular beam epitaxy growth of thin films of SnS$_2$ and SnSe$_2$. *Journal of Vacuum Science & Technology A* **13**, 1761–1767 (1995).

36. Zhao, Y. *et al*. Interlayer breathing and shear modes in few-trilayer MoS$_2$ and WSe$_2$. *Nano Lett.* **13**, 1007–1015 (2013).

37. Kim, K., Lee, J.-U., Nam, D. & Cheong, H. Davdov splitting and excitonic resonance effect in Raman spectra of few-layer MoSe$_2$. *ACS Nano* **10**, 8113–8120 (2016).

38. Froehlicher, G. *et al*. Unified description of optical phonon modes in N-layer MoTe$_2$. *Nano Lett.* **15**, 6481–6489 (2015).

39. Yang, J., Lee, J.-U. & Cheong, H. Excitation energy dependence of Raman spectra of few-layer WS$_2$. *FlatChem* **3**, 64–70 (2017).

40. Lorchat, E., Froehlicher, G. & Berciaud, S. Splitting of interlayer shear modes and photon energy dependent anisotropic Raman response in N-layer ReSe$_2$ and ReS$_2$. *ACS Nano* **10**, 2752–2760 (2016).

41. Zhao, Y. *et al*. Interlayer vibrational modes in few-quintuple-layer Bi$_2$Te$_3$ and Bi$_2$Se$_3$ two-dimensional crystals: Raman spectroscopy and first-principle studies. *Phys. Rev. B* **90**, 245428 (2014).

42. Luo, X. *et al*. Large frequency change with thickness in interlayer breathing mode—Significant interlayer interactions in few layer black phosphorus. *Nano Lett.* **15**, 3931–3938 (2015).

43. Tan, P. H. *et al*. The shear mode of multilayer graphene. *Nature Materials* **11**, 294–300 (2012).

44. Lui, C. H., Ye, Z., Keiser, C., Xiao, X. & He, R. Temperature activated layer breathing vibrations in few-layer Graphene. *Nano Lett.* **14**, 4615–4621 (2014).

45. Luo, X. *et al*. Stacking sequence determines Raman intensities of observed interlayer shear modes in 2D layered materials—A general bond polarizability model. *Scientific Reports* **5**, 14565 (2015).

46. Chen, J. M. & Wang, C. S. Second order Raman spectrum of MoS$_2$. *Solid State Comm.* **14**, 857–860 (1974).

47. Julien, C., Mavi, H. S., Jain, K. P. & Balkanski, M. Resonant Raman studies of SnS$_2$ crystals. *Material Science and Engineering B* **23**, 98–104 (1994).

48. Zhang, X. *et al*. Phonon and Raman scattering of two-dimensional transition metal dichalcogenides from monolayer, multilayer to bulk material. *Chem. Soc. Rev.* **15**, 2757–2785 (2015).

49. Lu, X., Luo, X., Zhang, J., Quek, S. Y. & Xiong, Q. Lattice vibrations and Raman scattering in two-dimensional layered materials beyond graphene. *Nano Research* **9**, 3559 (2016).

Acknowledgements

Author Contributions

H.C. conceived the experiments. T.S. and K.K. carried out measurements. All authors analyzed the data and wrote the manuscript.

Additional Information

Supplementary information accompanies this paper at https://doi.org/10.1038/s41598-018-28569-6.

Competing Interests: The authors declare no competing interests.

Publisher's note: Springer Nature remains neutral with regard to jurisdictional claims in published maps and institutional affiliations.